Available online at www.sciencedirect.com
SCIENCE DIRECT®
Journal of Nuclear Materials 348 (2006) 51–59
journal of nuclear materials
www.elsevier.com/locate/jnucmat

Theoretical study of helium insertion and diffusion in 3C-SiC

Renée M. Van Ginhoven [a], Alain Chartier [a,*], Constantin Meis [b], William J. Weber [c], L. René Corrales [c]

[a] CEA-Saclay DEN/DPC/SCP, Bât. 450Sud, 91191 Gif-Sur-Yvette, France
[b] INSTN-Saclay UEPEM, 91191 Gif-Sur-Yvette, France
[c] Pacific Northwest National Laboratory, P.O. Box 999, Richland, WA 99352, USA

Received 29 November 2004; accepted 2 September 2005

Abstract

Insertion and diffusion of helium in cubic silicon carbide have been investigated by means of density functional theory. The method was assessed by calculating relevant properties for the perfect crystal along with point defect formation energies. Results are consistent with available theoretical and experimental data. Helium insertion energies were calculated to be lower for divacancy and silicon vacancy defects compared to the other mono-vacancies and interstitial sites considered. Migration barriers for helium were determined by using the nudged elastic band method. Calculated activation energies for migration in and around vacancies (silicon vacancy, carbon vacancy or divacancy) range from 0.6 to 1.0 eV. Activation energy for interstitial migration is calculated to be 2.5 eV. Those values are discussed and related to recent experimental activation energies for migration that range from 1.1 [P. Jung, J. Nucl. Mater. 191–194 (1992) 377] to 3.2 eV [E. Oliviero, A. van Veen, A.V. Fedorov, M.F. Beaufort, J.F. Bardot, Nucl. Instrum. Methods Phys. Res. B 186 (2002) 223; E. Oliviero, M.F. Beaufort, J.F. Bardot, A. van Veen, A.V. Fedorov, J. Appl. Phys. 93 (2003) 231], depending on the SiC samples used and on helium implantation conditions.

PACS: 71.15.Mb; 61.72.Vv; 66.30.Jt

1. Introduction

Silicon carbide (SiC) has high chemical and thermal stability. In addition, SiC has good resistance to neutron radiation damage [4,5], and because of low cross-section for neutron capture, this material exhibits low induced activity from exposure in neutron irradiation environments. As a result of these properties, SiC is an important candidate material for components in nuclear fusion reactors [6–8] and as encapsulating material for nuclear fuel in light water reactors [9] and gas-cooled fission reactors [10,11]. As a wide band gap semiconductor, SiC also has potential use for sensors in nuclear power reactors [12].

In a fission or fusion nuclear environment, SiC components will be subject to a high flux of energetic neutrons, transmutations and helium accumulation from nuclear reactions [13]. In a fusion

* Corresponding author. Tel.: +33 1 6908 3168.
E-mail address: achartier@carnac.cea.fr (A. Chartier).

0022-3115/$ - see front matter
doi:10.1016/j.jnucmat.2005.09.006

reactor environment, helium generation rates from nuclear reactions in SiC can be relatively large [14]. Helium is also a proposed coolant gas for high temperature gas-cooled reactors [10,11], and interactions of the neutron flux with the coolant gas results in a low flux of He [15] that can lead to He implantation at surfaces. In electronic and optoelectronic device applications, implantation of light particles, such as helium, is a means of introducing controlled (desired) defect sites or regions with altered structure, such as gettering sites [16].

Helium accumulation in SiC produces changes in mechanical [13] and dimensional stability, since the helium promotes the growth of voids [17]. In order to predict performance of SiC materials under reactor operating conditions, mechanisms for these changes must be understood. Therefore, studies of release and retention behavior of helium in this material are required to assess performance and enable design of devices. There have been many experiments performed on helium-implanted silicon carbide samples. Typically, studies are done after helium implantation in polycrystalline samples, so that the sample has experienced significant damage from the implantation process. Simulations of collision cascade processes have shown that the largest proportion of surviving defects are isolated point defects, either single vacancies or interstitial atoms [18]. Due to the relative ease in displacement, (20 eV for C, 35 eV for Si) many more carbon defects are produced than silicon defects [19,18]. Both simulation and irradiation experiments indicate that at low doses, damage to the carbon sublattice dominates [20], while at higher doses, the proportional damage to the silicon lattice increases [21]. This is consistent with a higher rate of C Frenkel pair recombination [22] and the higher mobility of interstitial carbon [23]; the C sublattice has a faster rate of damage recovery. In addition, intrinsic vacancy-type defects that have been proposed include isolated silicon and carbon vacancies, divacancies [24] and the carbon vacancy–carbon antisite pair [26,27].

In helium-implanted and neutron-irradiated samples, depending on implantation doses and post-irradiation annealing temperatures, helium has been observed to be trapped in the grain interior as two-dimensional disks of bubbles in the close packed direction, i.e. in habit planes (0 0 0 1) in 4H-SiC and (1 1 1) in 3C-SiC [28]. It has also been observed in depleted zones near grain boundaries or as faceted bubbles along them [29]. Experiments do not provide direct evidence for single helium atoms trapped in interstitial sites or in vacancies. However, the presence of large amounts of helium has significant effects on the evolution of microstructure during irradiation, leading to the formation of bubbles and dislocation loops in the interior of grains [29,30].

Helium migration is determined experimentally by observations of bubble migration or coarsening, and by thermal desorption studies. Jung [1] showed that helium atoms implanted in α-SiC migrate over macroscopic distances with an activation energy of about 1.1 eV, with an assumed 'dissociative mechanism' that is a sequence of trapping and detrapping in irradiation-induced vacancies coupled with interstitial diffusion. In experiments measuring thermal desorption of helium from low-energy implanted SiC, Oliverio et al. [2,3] found two desorption ranges, with actual characteristics dependant on sample preparation and history. The helium desorption spectra for both 4H-SiC and 6H-SiC showed two peaks, centered at 600 and 1200 K. The underlying mechanisms are estimated to have activation barriers of 1.5 and 3.2 eV. Helium desorption peaks in polycrystalline cubic SiC grown by vapor deposition were found at 600 and 1000 K with estimated activation energy 1.5 and 2.7 eV, respectively. Each release stage appeared to have multiple peaks, and these were subject to shifts in relative intensity and temperature range depending on the nature and history of the sample in question. For high concentrations of helium, complex behavior is seen, involving dislocation loops and bubble growth consistent with an Ostwald ripening process influenced by pressure and repulsion between defects. Energy barriers for these more complicated processes are in the range of 3.5–4.4 eV [29,30].

Finally, helium behavior in 3C-SiC is strongly dependant on its association with irradiation-induced defects and the helium diffusion pathways for which little is known at the microscopic scale. The present work is therefore focused on helium insertion and relaxation into interstitial positions or into vacancies, and helium migration into and out of vacancy sites. We examine the atomic level configuration and stability of inserted helium and the mechanism of helium diffusion in silicon carbide, using density functional theory (DFT). We take advantage of recent theoretical studies [23,31–33] on migration of intrinsic defects in 3C-SiC, that give microscopic details on experimental values.

The DFT method is applied to the perfect 3C-SiC structure. Some intrinsic point defects are investi-

gated and the results compared with other theoretical studies in order to assess the method. Insertion of helium in interstitial sites is also carefully examined. Next, a detailed study of helium insertion in different sites and determination of migration pathways are presented. Finally, results are discussed and linked with available experimental data.

2. Simulation methods

Silicon carbide crystallizes into many different configurations: more than 250 different polytypes have been reported up to now [34]. 3C-SiC (cubic), 4H-SiC and 6H-SiC (hexagonal) are the most commonly studied since they represent the main polytypes of interest for applications. The local bonding characteristics are the same for all polytypes: silicon (carbon) forms covalent sp^3 bonds with four other carbon (silicon), building a network of alternating silicon and carbon centered tetrahedra. The main difference between polytypes is the stacking of Si and C planes along the $\langle 1\,1\,1\rangle$ in 3C-SiC and along the *c*-axis in 4H and 6H-SiC. The stacking sequence is ABC in the 3C-SiC cubic phase, and ABCACB in the hexagonal 6H-SiC polytype. We study here the more symmetric cubic phase 3C-SiC ($F\bar{4}3m$ space group). Carbon is located in the 4*a* (0, 0, 0) special site, while silicon is in the 4*c* (1/4, 1/4, 1/4) site, both having the $\bar{4}3m$ site symmetry.

The present study was carried out using the density functional theory (DFT) method implemented in the NWChem code [35]. The DFT calculations were performed using pseudopotential-plane waves in the local density approximation (LDA), using the Vosko [36] exchange-correlation functional. The valence–core interactions were represented by the norm-conserving pseudopotentials developed by Hamman [37] modified to a separable form as described by Kleinman and Bylander [38] for silicon, carbon and helium. A softer parametrization was used for carbon [39] to reduce the required number of plane waves. Cluster calculations of carbon have shown that the softer pseudopotential is reliable [40–42]. A plane-wave basis with a cutoff of 36 Ry was used for all calculations since previous work on silicon carbide has shown this to be sufficient [39]. Due to the large number of calculations required to calculate full migrations paths (described below), only the Γ point for the Brillouin-zone integration has been considered in this work.

Optimization of the 3C-SiC cell volume with DFT-LDA was performed on an eight-atom unit cell with periodic boundary conditions. Atoms positions were first optimized using a Broyden–Fletch–Goldfarb–Shanno quasi-Newton algorithm with analytic gradients at different fixed volumes. Structural optimizations were subject to a convergence criterion of 10^{-4} a.u. The optimized unit cell was obtained by fitting the Birch–Murnaghan equation of state [43] (with B' fixed to the experimental value 4) to the resulting calculated energy versus volume curve. Calculated structural values are shown in Table 1. The cell parameter *a* is slightly overestimated compared to the experimental value. This is likely due to the use of a soft parametrization of the carbon pseudopotential in combination with the integration only on the Γ point in the reciprocal space. The difference between the experimental and the calculated value is small and shows the same trend as found recently by Ziambaras and Schröder [44]. The cohesive energy (E_{coh}) was calculated using the difference between the perfect crystal and single atoms gas phase energies, as stated by the following equation:

$$E_{coh} = E(SiC) - E(Si_{gas}) - E(C_{gas}). \quad (1)$$

Calculations for single atoms (C_{gas} or Si_{gas}) were performed for the triplet state in a fcc cell with a lattice constant of 38 a.u. and the same energy cutoff as for the crystal. No correction for vibrational energy has been introduced in our calculation. The calculated E_{coh} obtained with the eight-atom cell is 7.32 eV (see Table 1).

Minimum energy paths (MEP) for atom migration were determined using the nudged elastic band – climbing image method (NEB-CI) applied

Table 1
Comparison between experimental [29,56,57] and calculated structural values with the Birch–Murnaghan equation of state [43] within the DFT-LDA method for the eight-atoms cell of 3C-SiC

	Present calc.	Ref. [44]	Exp.
a (Å)	4.38	4.376	4.3581
d(SiC) (Å)	1.898		1.887
B (GPa)	218	213	224
B' (fixed)	4.0	3.93	4.0
E_{coh} (eV/atom)	7.32		6.5

E_{coh} is the cohesive energy and is calculated using Eq. (1). Ab initio calculations done by Ziambaras and Schröder [44] have been quoted for comparison.

to the DFT potential energy surface. Briefly, the NEB method works as follows. A chain of images is generated between two minima on a potential energy surface, by extrapolating the coordinates of the atoms from one minima to another. Neighboring images interact via a harmonic potential along the direction of the path described by the chain, and the forces on the ions are further modified such that the original system forces parallel to the path and the inter-image spring forces perpendicular to the path are removed. The entire chain is then relaxed as a unit. The saddle point geometry is refined using the climbing image method, which works by inverting the parallel force on images that are higher in energy than either of their neighbors. This method robustly finds a saddle point on a given path, given that there are sufficient images to describe the path topology. Further details about this method may be found in Refs. [50–52]. All diffusion paths were determined using a 64-atom cubic supercell at the fixed optimized volume. For relatively simple paths, a chain of five images was sufficient to converge to an acceptable approximation to the transition state. For paths involving concerted motion, up to ten images were used. The initial images were obtained by a simple linear extrapolation between adjacent minima. Structural optimizations involved in that procedure were subject to a convergence criterion of 10^{-3} a.u. for the sum of the force over the full chain.

The geometry of the NEB image chains was optimized using a modified steepest descent method in which the velocity is zeroed when the force changes sign. Experience with NEB calculations [53] has shown that the stability of this approach is often required.

3. Results

3.1. Intrinsic point defects: evaluation of the method

The formation energy of intrinsic point defects were calculated and compared with other theoretical results. This work is focused on vacancies, where helium is expected to stabilize. Vacancies were formed by the removal of C and/or Si atoms and all of the associated electrons, so that the simulation cell is electrically neutral. Consequently, no Madelung correction was needed. All defect calculations were done using a 64-atom supercell (unless otherwise specified), with the volume fixed at the optimal value as determined for the perfect crystal above. Positions of all atoms were relaxed without symmetry constraints. In the following, the carbon (silicon) neutral vacancy is described by the notation V_{C} (V_{Si}), unless otherwise specified. The notation $V_{\mathrm{C}}V_{\mathrm{Si}}$ represents a divacancy, where vacancies are first neighbors. The $V_{\mathrm{C}}\mathrm{C}_{\mathrm{Si}}$ represents a carbon antisite adjacent to a carbon vacancy.

Defect formation energies were calculated as the difference in total atomization energy for the perfect and defective systems, corrected for the cohesive energy (E_{coh} calculated using Eq. (1)) of the removed atom. For example, the defect formation energy of a single carbon vacancy is defined as

$$E_{\mathrm{f}}(V_{\mathrm{C}}) = E(\mathrm{Si}_{32}\mathrm{C}_{31}) + E(\mathrm{C}_{\mathrm{gas}}) - E(\mathrm{Si}_{32}\mathrm{C}_{32}) - E^{A}_{\mathrm{coh}}(\mathrm{SiC}) + 1/2(E^{A}_{\mathrm{coh}}(\mathrm{C}) - E^{A}_{\mathrm{coh}}(\mathrm{Si})). \quad (2)$$

This definition is consistent with the one used by Posselt et al. [45]. $E^{A}_{\mathrm{coh}}(\mathrm{SiC})$ sets for the atomic cohesive energy of SiC, while $E(\mathrm{Si}_{32}\mathrm{C}_{31})$ and $E(\mathrm{Si}_{32}\mathrm{C}_{32})$ are the total energies calculated with and without defect. The last term of Eq. (2) is also set to 1.37 eV, which is half the difference of the Si and C experimental cohesive energy E^{A}_{coh} [46,47]. Note that the last term of Eq. (2) is removed for $V_{\mathrm{C}}\mathrm{C}_{\mathrm{Si}}$ defects, and null for divacancy $V_{\mathrm{Si}}V_{\mathrm{C}}$.

Selected calculations were performed using a 128-atom unit cell, in order to check the effect of the cell size. Calculated defect formation energies are given in Table 2. The present results (with 128 atoms) are comparable with those obtained by Torpo et al. [24] using the same size cell and the Γ k-point only. Comparison of present results using 64-atom and 128-atom supercells show that the formation energy of the silicon vacancy is more affected by the cell size than the other vacancy configurations, with a variation of about 6.1%. The other formation energies have variations of less than 3%.

3.2. Helium insertion in perfect and vacancy containing SiC

Insertion of helium in SiC was calculated using the 64-atom supercell in the DFT-LDA, with the helium gas phase chosen as a reference. Thus, insertion energy in an interstitial site is calculated according to the following relation:

$$E_{\mathrm{ins}}(\mathrm{He}_{\mathrm{interstitial}}) = E(\mathrm{Si}_{32}\mathrm{C}_{32} + \mathrm{He}_{\mathrm{interstitial}}) - E(\mathrm{Si}_{32}\mathrm{C}_{32}) - E(\mathrm{He}_{\mathrm{gas}}). \quad (3)$$

Table 2
Formation energies of neutral vacancies in 3C-SiC, calculated as described by Eq. (2)

Ref.	Present calculations		[24]	[33]	[49]	[48]
PP	BHS	BHS	Vanderbilt	TM	TM	Vanderbilt
Cutoff (Ry)	36	36	20	36	36	13
k-set	Γ	Γ	Γ	Γ	2^3	4^3
Supercell	64	128	128	216	128	216
V_C	3.47	3.54	2.77	4.1	4.80	4.30
V_{Si}	7.62	7.16	7.79	8.0	8.45	8.69
$V_C C_{Si}$	5.72	5.44				
$V_{Si} V_C$	7.32	7.23	7.22			

V_C and V_{Si} are carbon and silicon vacancies, respectively. $V_{Si}V_C$ indicates a divacancy while $V_C C_{Si}$ is a carbon vacancy–carbon antisite defect pair. Formation energies taken from previous ab initio works have been made consistent with the current definition of Eq. (2), in agreement with Ref. [45].

In cubic SiC, there are two possible different interstitial locations for a helium atom. The helium interstitial may sit in the 4*b* (1/2, 1/2, 1/2) special site, labeled as T_{Si} in Table 3 with the $\bar{4}3m$ site symmetry which is surrounded by four silicon atoms, or the 4*d* (3/4, 3/4, 3/4) special site, labeled T_C, with the same site symmetry, and which is surrounded by four carbon atoms.

For insertion of helium in vacancy sites, vacancy containing 64-atom supercells are used. The insertion energies are obtained from (example is for a carbon vacancy)

$$E_{ins}(\mathrm{He}(V_C)) = E(\mathrm{Si}_{32}\mathrm{C}_{31} + \mathrm{He}(V_C)) - E(\mathrm{Si}_{32}\mathrm{C}_{31}) - E(\mathrm{He}_{gas}). \quad (4)$$

Different configurations have been considered and labelled with respect to the center of the silicon or carbon vacancy, and for the carbon-vacancy-antisite defect. The site called *center* in Table 3 denotes a helium inserted just at the coordinates of the removed atom, that is silicon for V_{Si} or carbon for V_C. The NN notation sets for helium inserted in the nearest neighbor interstitial sites, which are inside the vacancy space. The T_C and T_{Si} labels for NN configurations, indicate the initial position of a helium atom before relaxation. After relaxation, helium atoms which begin within the void space are displaced slightly, towards the center of the vacancy site. The position of the helium atom also affects the relaxation of the under-coordinated atoms surrounding the vacancy, generally pushing the nearby atoms slightly outward. Helium atoms were also inserted in next nearest neighbour interstitial sites, designated NNN, which are interstitial positions adjacent to the vacancy.

Calculated insertion energies E_{ins} for all the configurations have been reported in Table 3. Helium insertion energy in interstitial sites is relatively high 1.51 eV in T_{Si} and 2.71 eV in T_C sites, respectively. These values are lower in energy compared with neutral C and Si interstitial formation energies, between 6 and 7 eV [25]. Detailed analysis of the electron density shows interactions between helium and carbon/silicon atoms are purely repulsive, with no apparent polarization of the helium. The higher

Table 3
Summary of helium insertion energies E_{ins} in interstitials, vacancies and close to vacancies (as defined by Eqs. (3) and (4))

(eV)	V_C		V_{Si}				$V_C C_{Si}$		$V_C V_{Si}$		Interstitials	
Sites									V_C	V_{Si}	T_C	T_{Si}
E_{ins} (center)	1.62		0.86				0.91		0.95	0.45	2.71	1.51
Sites	T_C	T_{Si}	T_C	T_{Si}	T_C	T'_{Si}	T_{C-C}	T_{Si_3C}				
E_{ins} (NN)	1.57	1.46	0.88	0.57	1.57	2.03	2.17	1.13				
E_{ins} (NNN)	2.74	1.53	2.73	1.47	2.70	1.73	1.91	2.68				
E_f	3.47		7.62				5.72		7.32	7.32	–	–
$E_{tot.}$	5.09		8.48				6.63		8.27	7.77	2.71	1.51

Total insertion energies E_{tot} have been calculated by the sum of formation energies of vacancies E_f (as defined by Eq. (2) and quoted Table 2) and the insertion energies E_{ins}(center) of helium in the centered sites.

insertion energy for the T_C site may be explained by the fact that the void space available for helium is smaller and more rigid. The relative electronegativity of carbon versus silicon favors excess electron density on the C atoms thus, steric repulsion is increased in that void space.

Table 3 shows that insertion energies of helium in *center* and NN sites close to the silicon vacancy are lower than insertion energies at equivalent sites close to the carbon vacancy. For both V_C and V_{Si} sites, helium insertion is more favorable in T_{Si} sites in NN or NNN positions than in corresponding T_C sites. This result is consistent with the previously noted trend for interstitials. It is interesting that NNN insertion energies are very close to insertion in interstitial sites without any nearby vacancy (Table 3, interstitials column). This means that the helium–vacancy interaction is very low for distances longer than 3.7 Å. The insertion energy for helium in a center versus an NN site is not significantly different.

For the carbon vacancy–carbon antisite defect, V_CC_{Si}, additional notations are necessary due to the removal of the site symmetry. Thus, $T_{C–C}$ and T_{Si_3C} indicate T_C and T_{Si} sites in which one of nearest silicon atoms is replaced by a carbon atom. The vacancy space for those defects are distorted as compared to an isolated carbon vacancy. For a $T_{C–C}$, this distortion induces a relative compression in the interstitial spaces, leading to insertion energies higher than for an undistorted carbon vacancy, see Table 3. For T_{Si_3C}, the distortion due to the carbon antisite creates a slightly larger space than what is available in the carbon vacancy, so that insertion energy of helium in the NN zone (1.13 eV) is close to the value obtained in the *center* site (0.91 eV). Conversely, there is no influence on insertion energy (compared to the V_C–T_C) for the V_CC_{Si}–T_C, which is the site on the face across the antisite. The three sites V_CC_{Si}–T'_{Si}, adjacent to this face have insertion energies slightly changed compared with a regular V_C–T_{Si} site, but that difference is significant only for the NN configuration.

3.3. Helium migration in 3C-SiC

The mechanism for helium migration most likely involves escape from a vacancy site, and then eventually interstitial diffusion. Interstitial migration through the interior of a defect-free crystal consists of alternating paths between adjacent T_{Si} and T_C sites. Five images were used to find the interstitial MEP using the NEB method. The resulting path is shown in Fig. 1. The activation energy for migration from the T_{Si} to the T_C is calculated as the difference in energy between the cell where helium is at the saddle point and the cell where helium is at the T_{Si} site. The resulting value is 2.5 eV for helium migration from T_{Si} to T_C. The reverse path has a barrier of 1.3 eV (see Table 4). The activation energies for migration are high when compared to those obtained for C or Si interstitial migration (around 1.5 eV [33]). This is due to the fact that the helium does not create bonds and consequently has to push out the lattice atoms to pass from one interstitial site to the other. Finally, the higher activation energy for helium migration (2.5 eV) is the rate limiting factor for migration via interstitial sites only, which is thought to be the long-range migration pathway within a single crystal. For helium migration in

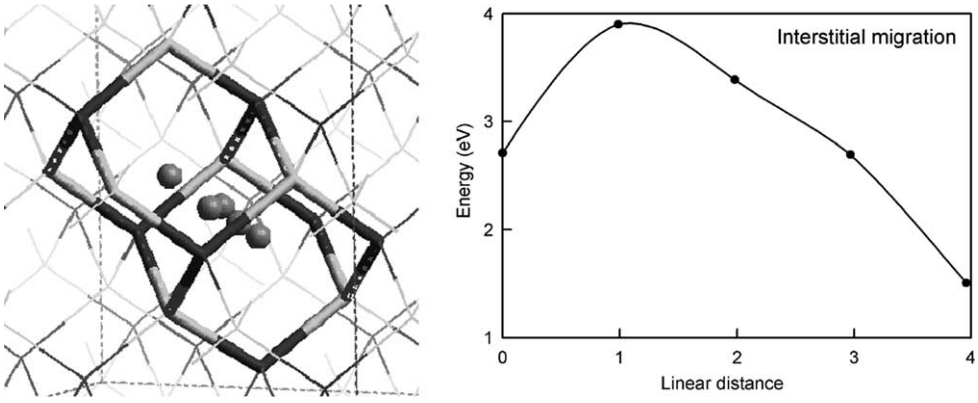

Fig. 1. Interstitial migration of a helium atom in silicon carbide. The direction $T_C \rightarrow T_{Si}$ runs from left to right. Silicon (carbon) atoms are shown in light (dark) grey sticks, while helium is represented by spheres. All five sets of NEB image coordinates are shown superimposed.

Table 4
Activation energies for helium migration in cubic silicon carbide obtained by using the NEB method

Migration path	Barrier (reverse) (eV)	
	V_C	V_{Si}
Center → T_CNN	0.6 (0.6)	–
T_CNN → T_{Si}NN	0.9 (1.0)	0.0 (0.4)
T_CNN → T_{Si}NNN	2.3 (2.3)	2.6 (2.0)
T_{Si}NN → T_CNNN	2.1 (0.8)	3.4 (1.3)
Divacancy		
V_CC → $V_{Si}C$	0.2 (0.7)	
Interstitial		
T_C → T_{Si}	1.3 (2.5)	
V_{Si} → V_CC_{Si}	3.0 (4.9)	
V_{Si} + (He *center*) → V_CC_{Si} + (He T_{Si_3C})	3.0 (4.6)	

The overall de-trapping barrier is 2.1 eV for a carbon vacancy and 2.9 eV, for a silicon vacancy. Two last lines show activation energies for formation of complex form a silicon vacancy, with and without helium present. Both paths are shown in Fig. 3.

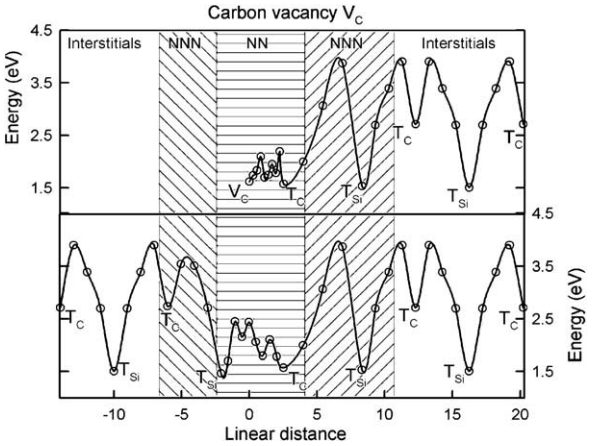

Fig. 2. Minimum energy paths (MEP) calculated using the NEB method [50–52] as a function of the linear distance along the paths for helium migration out of the carbon vacancy. An arbitrary zero has been taken for the *center* site. The upper part of the figure represents the full migration path from the *center* to interstitial sites, that is representative of a 'dissociative mechanism'. The lower part represents migration paths from NN T_C and T_{Si} sites toward interstitial sites. Three different zones have been distinguished. The NN zone contains migration paths between the *center* and the NN T_C and T_{Si} sites. The NNN zone contains migration paths between NN sites and NNN sites. Finally, the interstitial zone contains migration paths between interstitial sites.

and around vacancies, the carbon vacancy is considered first for a detailed description of the paths. According to the carbon vacancy site symmetry ($\bar{4}3m$), four equivalent paths can lead helium from the *center* site to the NN T_{Si} and four others to the NN T_C sites. Twelve equivalent paths exist for the migration between NN T_{Si} and NN T_C sites. The corresponding MEP's optimized within the NEB method as a function of the linear distance along the paths are shown in Fig. 2. The V_C to T_{Si} path has not been represented since after optimization it was found that helium passes through the T_C site before reaching the T_{Si} site. Three different zones can easily be distinguished in Fig. 2. The NN zone corresponds to migration of helium between *center* and NN sites. The NNN zone corresponds to the migration between NN and NNN sites. Finally, the migration between interstitial sites has been shown again, for direct comparison with migration in the NN and NNN zones. Activation energies between NN and NNN sites are similar (2.1–2.3 eV, see Table 4) to activation energies for interstitial migrations (2.5 eV). Migration barriers inside the carbon vacancy are around one third lower, that is between 0.6 and 1.0 eV (see Table 4), with unexpectedly complicated path topology. Paths between V_C and T_C, or between T_C and T_{Si}, appear to pass through several intermediate metastable configurations (see Fig. 2). This results from quite small geometrical reorganizations of the immediately surrounding 3C-SiC lattice. For the path between V_C and T_C, the overall migration energy is about 0.6 eV. This rather low value allows helium to reorganize inside the vacancy. Migration barriers along the borders of the vacancy, i.e. between T_C and T_{Si}, are around 0.9 eV. Migration barriers for a helium associated with a simple silicon vacancy are also shown in Table 4. Compared to the carbon vacancy, hopping around inside the vacancy has lower barriers (0.4 eV), while exit barriers are higher (2.6 eV).

For carbon and silicon vacancies results show low activation energies (0.4–1.0 eV) for helium migration in and around vacancies. These values may be related to the activation energy of 1.1 eV obtained by Jung and Oliviero et al. [1,28] and correspond to helium migration along grain boundaries that contain a significant population of vacancies. Oliviero et al. [2,3] attributed a value of 3.2 eV for helium detrapping from vacancy sites in mono-crystalline 4H-SiC and for CVD-3C-SiC. That value is related to values around 2.5 eV obtained in the present work for helium dissociation from silicon as well as carbon vacancies.

Investigation of the silicon vacancy is complicated by the fact that it is expected to convert to a V_CC_{Si} defect. To create the vacancy–antisite pair, one of the 3-fold coordinated carbon atoms

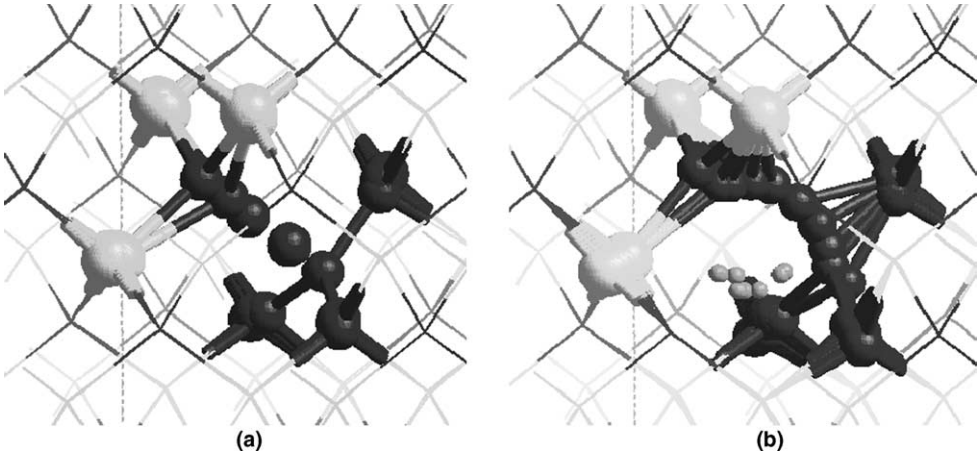

Fig. 3. MEP for formation of the V_CC_{Si} defect from a silicon vacancy (a) without, and (b) with a helium atom present. The atoms that are directly involved in the migration process are shown as spheres, with carbon in black, and silicon in light grey. The helium (when present) atom is shown as a small sphere in medium grey. The surrounding lattice is shown in stick representation. Five path images are superimposed in (a), and all ten images are shown for the concerted carbon/helium motion in (b).

adjacent to the empty site moves directly across the vacancy to occupy the empty silicon lattice site. In the configuration containing helium, the helium atom was moved between the lowest energy insertion site for each defect type, from the *center* of V_{Si}, to the closest T_{Si_3C} site of the V_CC_{Si} endpoint. The atomic positions for both MEP's are shown in Fig. 3. The presence of a helium atom stabilizes the simple silicon vacancy slightly with respect to the V_CC_{Si}, by about 0.3 eV. However, despite the obvious difference in the path character, the barrier for the formation of the vacancy–antisite pair from the silicon vacancy remained unchanged with or without helium, at 3.0 eV (see Table 4). This value is higher than the experimental determined activation energy of about 2.2 eV for the annealing process for the silicon vacancy observed by Itoh and Hayakawa [54] but close to that of 3.1 eV obtained by Balona et al. [55]. A range of values have been obtained theoretically: 1.8 eV by Rauls [31], and 2.4 ± 0.3 eV for the neutral defects by Bockstedte et al. [33], and also 2.35 eV by Gao et al. [23].

Acknowledgements

W.J.W. was supported by the Division of Materials Sciences and Engineering, Office of Basic Energy Sciences, US Department of Energy, at the Pacific Northwest National Laboratory. L.R.C. was supported by the Division of Chemical Sciences, Office of Basic Energy Sciences, Department of Energy. Some of these calculations were carried out at the William R. Wiley Molecular Science Laboratory, a national scientific user facility sponsored by the Department of Biological and Environmental Research located at the Pacific Northwest National Laboratory. Pacific Northwest Laboratory is operated for the Department of Energy by Battelle. Part of these calculations were done at the Département de Physico-Chimie (CEA-Saclay). R.M.V., A.C. and C.M. were supported by DEN/DSOE (CEA-Saclay), and would like to thank G. Lozes and P. Chaix for grant prolongation.

References

[1] P. Jung, J. Nucl. Mater. 191–194 (1992) 377.
[2] E. Oliviero, A. van Veen, A.V. Fedorov, M.F. Beaufort, J.F. Bardot, Nucl. Instrum. and Meth. B 186 (2002) 223.
[3] E. Oliviero, M.F. Beaufort, J.F. Bardot, A. van Veen, A.V. Fedorov, J. Appl. Phys. 93 (2003) 231.
[4] H. Huang, N. Ghoniem, J. Nucl. Mater. 250 (1997) 192.
[5] D.J. Senor, G.E. Youngblood, L.R. Greenwood, D.V. Archer, D.L. Alexander, M.C. Chen, G.A. Newsome, J. Nucl. Mater. 317 (2003) 145.
[6] L. Giancarli, J.P. Bonal, A. Caso, G. Le Marois, N.B. Morley, J.F. Salavy, Fusion Eng. Des. 41 (1998) 165.
[7] Y. Ling, J. Li, C. Ge, X. Bai, J. Nucl. Mater. 303 (2002) 188.
[8] L.V. Boccaccini, U. Fischer, S. Gordeev, S. Malang, Fusion Eng. Des. 49&50 (2000) 491.
[9] Z. Alkan, K. Kugeler, R. Kaulbarsch, C. Manter, Progr. Nucl. Energy 38 (2001) 411.
[10] K. Minato, K. Sawa, K. Koya, T. Tomita, A. Ishikawa, C.A. Baldwin, W.A. Gabbard, C.M. Malone, Nucl. Technol. 131 (2000) 36.
[11] J.A. Lake, R.G. Bennett, J.F. Kotek, Sci. Amer. 286 (2002) 73.
[12] A.R. Dulloo, R.H. Ruddy, J.G. Seidel, J.M. Adams, J.S. Nico, D.M. Gilliam, Nucl. Instrum. and Meth. A 498 (2003) 415.

[13] L.L. Snead, R. Scholtz, A. Hasegawa, A. Frias Rebelo, J. Nucl. Mater. 307–311 (2002) 1141.
[14] J. Chen, P. Jung, Ceram. Int. 26 (2000) 513.
[15] F.A. Garner, C.W. Hunter, G.D. Johnson, E.P. Lippincott, J.O. Schiffgens, H. Farrar, Nucl. Technol. 58 (1982) 203.
[16] A. Declemy, E. Oliviero, M.F. Beaufort, J.F. Bardot, M.L. David, C. Blanchard, Y. Tessier, E. Ntsoenzok, Nucl. Instrum. and Meth. B 186 (2002) 318.
[17] R.J. Price, J. Nucl. Mater. 33 (1969) 17.
[18] F. Gao, W.J. Weber, Phys. Rev. B 63 (2000) 54101.
[19] F. Gao, W.J. Weber, Nucl. Instrum. and Meth. B 191 (2002) 487.
[20] W.J. Weber, F. Gao, W. Jiang, Y. Zhang, Nucl. Instrum. and Meth. B 206 (2003) 1.
[21] W.J. Weber, F. Gao, Nucl. Instrum. and Meth. 207 (2003) 10.
[22] F. Gao, W.J. Weber, J. Appl. Phys. 94 (2003) 4348.
[23] F. Gao, W.J. Weber, M. Posselt, V. Belko, Phys. Rev. B 69 (2004) 245205.
[24] L. Torpo, T.E.M. Staab, R.M. Nieminen, Phys. Rev. B 65 (2002) 85202.
[25] J.M. Lento, L. Torpo, T.E.M. Staab, R.M. Nieminen, J. Phys.: Condens. Matter 16 (2002) 1053.
[26] T. Lingner, S. Greulich-Weber, J.M. Spaeth, U. Gerstman, E. Rauls, H. Overhof, Physica B 308–310 (2001) 625.
[27] T. Lingner, S. Greulich-Weber, J.M. Spaeth, U. Gerstman, E. Rauls, Z. Hajnal, T. Frauenheim, H. Overhof, Phys. Rev. B 64 (2001) 245212.
[28] P. Jung, H. Klein, J. Chen, J. Nucl. Mater. 283–287 (2000) 806.
[29] J. Chen, P. Jung, H. Trinkhaus, Phys. Rev. B 61 (2000) 12923.
[30] E. Oliviero, M.L. David, M.F. Beaufort, J. Nomgaudyte, L. Pranevicius, A. Declemy, J.F. Bardot, J. Appl. Phys. 91 (2002) 1179.
[31] E. Rauls, PhD thesis, Universtät Paderborn, Paderborn, 2003.
[32] M. Bockstedte, PhD thesis, Universtät Paderborn, Paderborn, 2003.
[33] M. Bockstedte, A. Mattausch, O. Pankratov, Phys. Rev. B 68 (2003) 205201.
[34] W. Wesch, Nucl. Instrum. and Meth. B 116 (1996) 305.
[35] R.A. Kendall, E. Aprà, D.E. Bernholdt, E.J. Bylaska, M. Dupuis, G.I. Fann, R.J. Harrison, J. Ju, J.A. Nichols, J. Nieplocha, T.P. Straatsma, T.L. Windus, A.T. Wong, Comput. Phys. Commun. 128 (2000) 260.
[36] S.H. Vosko, L. Wilk, M. Nusair, Can. J. Phys. 58 (1980) 1200.
[37] D.R. Hamann, Phys. Rev. B 40 (1989) 2980.
[38] K. Kleinman, D.M. Bylander, Phys. Rev. Lett. 48 (1982) 1425.
[39] F. Gao, E.J. Bylaska, W.J. Weber, L.R. Corrales, Phys. Rev. B 64 (2001) 245208.
[40] E.J. Bylaska, J.H. Weare, Phys. Rev. B 58 (1998) R7488.
[41] E.J. Bylaska, P.R. Taylor, R. Kawai, J.H. Weare, J. Phys. Chem. 100 (1996) 6966.
[42] E.J. Bylaska, R. Kawai, J.H. Weare, J. Phys. Chem. 113 (2000) 6096.
[43] J.P. Poirier, Introduction to the Physics of the Earth's Interior, Cambridge University, Cambridge, 1991.
[44] E. Ziambaras, E. Schröder, Phys. Rev. B 68 (2003) 64112.
[45] M. Posselt, F. Gao, W.J. Weber, V. Belko, J. Phys.: Condens. Matter 16 (2004) 1307.
[46] K.J. Chang, M.L. Cohen, Phys. Rev. B 35 (1987) 8196.
[47] J. Furthmüller, J. Hafner, G. Kresse, Phys. Rev. B 50 (1994) 15606.
[48] A. Zywietz, J. Furthmüller, F. Bechstedt, Phys. Rev. B 59 (1999) 15166.
[49] B. Araldi, A. Gali, P. Deák, J.E. Lowther, N.T. Son, E. Janzén, W.J. Choyke, Phys. Rev. B 63 (2002) 245202.
[50] G. Henkelman, B. Uberuaga, H. Jónsson, J. Chem. Phys. 113 (2000) 9978.
[51] G. Mills, H. Jónsson, G. Schenter, Surf. Sci. 324 (1995) 305.
[52] G. Mills, H. Jónsson, K. Jacobsen, Classical and Quantum Dynamics in Condensed Phases, World Scientific, Singapore, 1998.
[53] R.M. Van Ginhoven, PhD thesis, University of Washington, Seattle, 2002.
[54] H. Itoh, N. Hayakawa, J. Appl. Phys. 66 (1989) 4529.
[55] L.A. de Balona, J.H.N. Loubser, J. Phys. C 3 (1970) 2344.
[56] K. Sasaki, T. Yano, T. Maruyama, T. Iseki, J. Nucl. Mater. 179–181 (1991) 407.
[57] W.R. Allen, J. Nucl. Mater. 210 (1994) 318.